Effect of Crystallinity on Enthalpy Recovery Peaks and Cold-Crystallization Peaks in PET via TMDSC and DMA Studies

Yeong-Tarng Shieh,[1] Yu-Sheng Lin,[2] Yawo-Kuo Twu,[3] Hong-Bing Tsai,[4] Rong-Hsien Lin[5]

[1]*Department of Chemical and Materials Engineering, National University of Kaohsiung, Kaohsiung 811, Taiwan*
[2]*Department of Chemical and Materials Engineering, National Yunlin University of Science and Technology, Douliou, Yunlin 640, Taiwan*
[3]*Department and Graduate Program of Bioindustry Technology, Dayeh University, Changhua 515, Taiwan*
[4]*Department of Chemical Engineering and Materials Engineering, National Ilan University, I-Lan 260, Taiwan*
[5]*Department of Chemical and Material Engineering, National Kaohsiung University of Applied Sciences, Kaohsiung 807, Taiwan*

Received 6 May 2009; accepted 5 October 2009
DOI 10.1002/app.31570
Published online 23 December 2009 in Wiley InterScience (www.interscience.wiley.com).

ABSTRACT: Poly(ethylene terephthalate) (PET) sheets of different crystallinity were obtained by annealing the amorphous PET (aPET) sheets at 110°C for various times. The peaks of enthalpy recovery and double cold-crystallization in the annealed aPET samples with different crystallinity were investigated by a temperature-modulated differential scanning calorimeter (TMDSC) and a dynamic mechanical analyzer (DMA). The enthalpy recovery peak around the glass transition temperature was pronounced in TMDSC nonreversing heat flow curves and was found to shift to higher temperatures with higher degrees of crystallinity. The magnitudes of the enthalpy recovery peaks were found to increase with annealing times for samples annealed $\leq$30 min but to decrease with annealing times for samples annealed $\geq$40 min. The nonreversing curves also found that the samples annealed short times ($\leq$40 min) having low crystallinity exhibited double cold-crystallization peaks (or a major peak with a shoulder) in the region of 108–130°C. For samples annealed long times ($\geq$50 min), the cold-crystallization peaks were reduced to one small peak or disappeared because of high crystallinity in these samples. The double cold-crystallization exotherms in samples of low crystallinity could be attributed to the superposition of the melting of crystals, formed by the annealing pretreatments, and the cold-crystallizations occurring during TMDSC heating. The ongoing crystallization after the cold crystallization was clearly seen in the TMDSC nonreversing heat flow curves. DMA data agreed with TMDSC data on the origin of the double cold-crystallization peaks. © 2009 Wiley Periodicals, Inc. J Appl Polym Sci 116: 1334–1341, 2010

Key words: poly(ethylene terephthalate); enthalpy recovery peaks; cold-crystallization; temperature-modulated DSC; dynamic mechanical analysis

INTRODUCTION

Poly(ethylene terephthalate) (PET) is a commercial important polymer material and widely used in fibers, films, bottles, and plastics.[1] An amorphous PET can be easily obtained by quenching from the melt because of its slow crystallization. A semicrystalline PET can be obtained by a cold-crystallization (or annealing) at above the glass transition temperature from the amorphous glass or by a melt-crystallization (nonisothermal or isothermal) from the melt. As the properties of PET depend very much on the crystallinity and morphology, the crystallization and melting behavior of PET have always drawn attention to investigate.[2–21] In these many studies, the crystallinity and morphology of PET are clearly seen to be influenced by various factors such as orientation, thermal history, and crystallization conditions which include temperature, time, heating and cooling rates, isothermal and nonisothermal processes, pretreatment conditions, and so forth.

PET is a semirigid crystalline polymer having slow crystallization behavior; this usually results in a nonequilibrium state containing metastable crystals or imperfect crystals following cooling from the melt. Annealing of this polymer below the glass transition temperature, without affecting crystallinity,[22,23] would relax the polymer chains toward an equilibrium state and result in a decrease in enthalpy.[22–33] Annealing of this polymer above the glass transition temperature would induce

Correspondence to: Y.-T. Shieh (yts@nuk.edu.tw).
Contract grant sponsors: National Science Council of Taiwan.

crystallization. A subsequent heating of both annealed samples might result in enthalpy recovery in the glass transition region and cold crystallization at above the glass transition. The enthalpy recovery is visible as an endothermic peak usually at the higher temperature side of the T_g signal (a stepwise change in the heat flow), whereas the cold crystallization is visible as an exothermic peak during a conventional DSC heating scan.

Previous studies[2,5] found that three endotherms appeared during a subsequent DSC heating of an isothermally melt-crystallized PET, including the low endotherm attributed to early melting of secondary crystals, the middle endotherm attributed to melting of primary crystals, and the high endotherm attributed to final melting of the recrystallized species. The middle endotherm was always present but not always distinguishable from the standard DSC analysis. Temperature-modulated differential scanning calorimetry (TMDSC) was used to easily detect the presence of the middle endotherm in the isothermally melt-crystallized PEN and PEEK[22,34] and revealed that the middle endothermic peak corresponded to the melting of crystals originally present in the sample and the high endotherm was from the melting of the recrystallized species. The low endotherm in the isothermally melt-crystallized PEN and PEEK usually at a temperature a few degrees above the isothermal annealing temperature was proved to be from the melting of secondary crystals. Multiple melting peaks in an isothermally melt-crystallized PET were also reported by Avila-Orta et al.[10] but were attributed to slightly different origins. They[10] attributed the low endotherm to the melting of very thin secondary crystals, the middle endotherm to the melting of secondary crystals and partial melting of less stable primary crystals, and the high endotherm to the melting of the remaining stable primary crystals and the recrystallized crystals. Tan et al.[7] reported double melting peaks in the cold-crystallized PET during DSC heating. The melt obtained by heating the cold-crystallized PET to temperatures in between the low- and high-endothermic peaks was metastable and was able to recrystallize in the subsequent heating. Rastogi et al.[13] compared microstructure or morphology of the cold-crystallized PET and that of the melt-crystallized PET at the same temperature. For the same crystallization temperature and time, the melt-crystallization of PET was easier to give bigger size of crystals and higher degree of crystallinity than the cold-crystallization of PET. This study[13] clearly finds that the crystallization mechanism is different for either crystallization process. Androsch and Wunderlich[14] studied the rigid amorphous fraction (RAF) in an 117°C-cold-crystallized PET and subsequently annealed PET at higher temperatures as a function of crystallinity and crystal perfection. They found that the crystallinity and RAF both increase during the cold-crystallization. The subsequent annealing at higher temperatures caused an increase in crystallinity but a decrease in RAF due to crystal perfection.

According to these previous studies, most focused on the crystallization and melting behaviors of the melt-crystallized PET from the melt. Few studies focused on those of the cold-crystallized (or annealed) PET from the amorphous glass. Since conditions of the annealing pretreatments affect the initial crystallinity and, consequently, the final properties after subsequent crystallizations, the effects of these pretreatment conditions on the subsequent cold-crystallization and melting behavior during heating have to be known before a precise morphology or property can be obtained. In an attempt to know this, PET samples of various crystallinity are created by annealing the amorphous PET at a temperature in between T_g and T_m for various times. Intrinsic relations between these thermal pretreatments and properties (such as thermal and mechanical properties) may thus be investigated.

TMDSC, a relatively new calorimetric technique,[35–38] has been extensively used for studying the melting and crystallization behavior in polymer systems,[39] and it is widely accepted that it can supply additional information compared with conventional DSC. In TMDSC, a sample is linearly heated with a superimposed low frequency temperature oscillation resulting in a modulation in the heating profile. TMDSC analysis provides total heat flow, such as that from conventional DSC, and the heat capacity-related reversing heat flow. The nonreversing heat flow is obtained by subtracting the reversing heat flow from the total heat flow. The nonreversing process, at the time and temperature at which the measurement is made, is either irreversible or in some way kinetically hindered. The nonreversing heat flow signal contains contributions from processes that are reversible at frequencies lower than that chosen for the modulation. The reversing process during heating a polymer includes the glass transition and parts of the endothermic crystal melting, whereas the nonreversing process contains all exothermic events such as crystallizations, the endothermic enthalpy recovery, and parts of the endothermic crystal melting. Much of the complexity of TMDSC analysis originates from the contribution of the crystal melting to both reversing and nonreversing processes.[35] The reversing melting process includes the melting of the polymer chains or chain segments near or on high-melting crystals, and with negligible cooling, these molecules can nucleate and recrystallize on these existing unmelted crystals,[37,38] whereas the nonreversing melting process mostly originates from the complete melting of crystals.

In this work, enthalpy recovery peaks in the T_g region and double cold-crystallization peaks above T_g are observed in the annealed amorphous PET sheets at 110°C for various times and are investigated as a function of annealing time and crystallinity by a TMDSC and a dynamic mechanical analyzer (DMA). As the TMDSC analysis is able to separate the reversing and nonreversing events, it is thus a better technique than conventional DSC to see the enthalpy recovery peak and the ongoing crystallization behavior above the cold crystallization peaks and thereby to investigate into the effects of annealing time on the enthalpy recovery peak and the origin of the double cold-crystallization peaks in the annealed PET. DMA can provide data of dynamic mechanical properties such as storage modulus, loss modulus, and tan delta as a function of temperature for a sample. As cold crystallizations during the heating of the annealed PET would cause changes of these dynamic mechanical properties, DMA will also be used to accompany with TMDSC for this study.

EXPERIMENTAL

The amorphous poly(ethylene terephthalate) (aPET) sheets of 0.5 mm in thickness were obtained from Nan Ya Plastics Corp. (Taipei, Taiwan). The intrinsic viscosity of the aPET was 0.704 dL/g. The aPET sheets were annealed in an oven at 110°C for various times. The annealing time was from 10 to 1000 min. For the denotation of a sample, the aPET-110-40 denoted the aPET after annealing at 110°C for 40 min, whereas aPET-110-1000 denoted the aPET after annealing at 110°C for 1000 min, etc. The density of aPET and the annealed aPET samples was determined by a weighing device according to the principle of Archimedes. The weight fractional crystallinity (X_d, %) of a sample was determined by density data using eq. (1) as follows,

$$X_d = \frac{\rho_c}{\rho}\frac{(\rho - \rho_a)}{(\rho_c - \rho_a)} \quad (1)$$

where ρ is the measured density at 25°C of an annealed aPET sample, ρ_a is the density of the amorphous PET (aPET) and is taken as 1.333 g/cm^3 from literature,[6] and ρ_c is the density of the fully crystalline PET and is taken as 1.455 g/cm^3 as described in the literature.[40–42] The calculated X_d data of samples studied are tabulated in Table I. For comparison, the weight fractional crystallinity (X_c, %) of a sample was also determined by calorimetry data using eq. (2) as follows,

$$X_c\% = \frac{\Delta H_m + \Delta H_{cc}}{\Delta H_m^\circ} \times 100\% \quad (2)$$

The calorimetry data of a sample were obtained from the first heating scan at 10°C/min on a standard DSC (DSC Q100, TA Instruments, New Castle, DE) from 30 to 300°C to obtain the heat of the exothermic cold-crystallization (ΔH_{cc}) and the heat of the endothermic melting (ΔH_m). ΔH_m^o is the heat of melting of perfectly crystalline PET which is 135 J/g.[43,44]

The temperature-modulated differential scanning calorimetry (TMDSC) experiments were conducted on a DSC (DSC Q100, TA Instruments) applying the "heat only" mode by heating the sample at 2°C/min superposed with a temperature oscillation modulation with an amplitude of 0.32°C at a frequency of 1/min. The temperature modulation amplitude was small enough so that there was no significant local cooling. During TMDSC heating scans from 0 to 300°C, the glass transition (with enthalpy recovery endotherms), the exothermic cold crystallization peaks, and the endothermic melting peaks were observed, and the corresponding glass transition temperature (T_g), enthalpy recovery peak temperature (T_{er}), first and second cold-crystallization temperatures (T_{cc1},and T_{cc2}, respectively), the ongoing crystallization peak temperature (T_{oc}), and first and second melting temperatures (T_{m1},and T_{m2}, respectively) were obtained, for aPET and the annealed aPET samples. The dynamic mechanical properties of the samples were measured on a dynamic mechanical analyzer DMA (DMA 2980, TA Instruments) through a tensile mode. DMA analyses were conducted at a heating rate of 3°C/min from 30 to 200°C and at an oscillation frequency of 1 Hz with an oscillation amplitude of 15 μm.

RESULTS AND DISCUSSION

Table I lists the degrees of crystallinity of aPET and the annealed samples, calculated using the density data and calorimetry data. As can be seen in Table I, the density and the density-based weight-fractional crystallinity (X_d) of a sample increase with increasing annealing times. The samples with annealing times $\leq$30 min give rise to the density-based crystallinities of near zero but give the calorimetry-based crystallinities (X_c) of over 10%. This discrepancy can be attributed to the thermally induced crystallization during the DSC heating scan. This induced crystallization enhances the ΔH_m and thus the crystallinity as calculated by eq. (2). This finding reveals that the calorimetry method using a DSC is unable to provide correct measurements of low crystallinities in a semicrystalline polymer. The calorimetry-based X_c of aPET is unexpectedly higher than that of the sample annealed $\leq$30 min. This can be attributed to the presence of initial crystals in the annealed samples

TABLE I
The Measured Density, Weight Fractional Crystallinity (X_d[a] and X_c[b], Calculated from Density and Calorimetry Data, Respectively), Heats of Cold-Crystallization (ΔH_{cc}), and Heats of Fusion (ΔH_m), of Amorphous PET (aPET) and Annealed aPET (aPET-110-t) at 110°C for Various Times (t)

PET samples	Annealing temp. (°C)	Annealing time (min)	Density (g/cm^3)	X_d[a] (%)	ΔH_{cc} (J/g)	ΔH_m (J/g)	X_c[b] (%)
aPET	–	–	1.333	0	–24.7	47.8	17.1
aPET-110-10	110	10	1.333	0	–28.5	45.6	12.6
aPET-110-20	110	20	1.335	1.8	–27.3	46.0	13.8
aPET-110-30	110	30	1.336	2.7	–27.0	44.9	13.2
aPET-110-40	110	40	1.360	23.7	–9.5	49.3	29.5
aPET-110-50	110	50	1.364	27.1	–5.1	47.2	31.2
aPET-110-100	110	100	1.368	30.5	+1.4	47.5	36.2
aPET-110-200	110	200	1.371	33.1	+1.9	48.1	36.6
aPET-110-500	110	500	1.372	33.9	+2.1	47.0	36.4
aPET-110-1000	110	1000	1.372	33.9	+2.3	46.6	36.2

The calorimetry data were obtained by a conventional DSC analysis from the first heating scan at a rate of 10°C/min.
[a] Weight fractional crystallinity was calculated from density data using eq. (1).
[b] Weight fractional crystallinity was calculated from calorimetry data using eq. (2).

which serve as a nucleating agent and facilitate the cold-crystallization giving more exothermic heats (i.e., ΔH_{cc}). For samples annealed $\geq$40 min, the calorimetry-based X_c are always higher than the density-based X_d as can be also seen in Table I. For these samples annealed for long times, the thermally induced crystallization still occurs during the DSC heating scan and again enhances the ΔH_m, leading to an overestimated crystallinity. The calorimetry method (normally conducted at moderate or low heating rates) is thus not an appropriate method to analyze the crystallinity of a semicrystalline polymer, unless the crystallization can not be thermally induced during the DSC heating scan before melting. To inhibit the thermally induced crystallization, a very rapid heating scan may be applied.[12]

Figures 1–3 show TMDSC curves for aPET, aPET-110-40, and aPET-110-1000, respectively. Each figure contains curves of total, reversing, and nonreversing heat flows. All three samples show a glass transition temperature in the region of 70–85°C and a major melting peak at near 250°C in the total heat flow curves. The aPET and aPET-110-40 exhibit exothermic peak(s) in the region of 110–130°C, attributed to cold-crystallizations, whereas aPET-110-1000 exhibits a small endothermic peak at near 120°C. This small endotherm shifts to higher temperatures if the annealing temperatures are higher, as can be seen in Figure 4 for aPET-140-50 (this sample was obtained by annealing at 140°C for 50 min), for example, which exhibits a small endotherm at near 144°C. This finding suggests that the small endotherm, appeared at some degrees higher than the annealing temperature, arises from the melting of crystals which evolve from the annealing, with higher annealing temperatures giving bigger sizes of crystals and thus higher melting temperatures as discussed in the following. According to the secondary nucleation theory, the initial crystal thickness (l_c^*) is inversely proportional to the degree of supercooling ($\Delta T = T_m^0 - T_c$) as follows:[45,46]

$$1_c^* \cong \frac{2\sigma T_m^0}{\Delta H(T_m^0 - T_c)} \tag{3}$$

where σ is the fold surface free energy, T_m^0 is the equilibrium melting temperature, ΔH is the heat of fusion per unit volume, and T_c is the crystallization (annealing) temperature. The sizes of crystals evolved from higher annealing temperatures are thus bigger than those from lower temperatures because the higher annealing temperatures give the smaller degrees of supercooling (ΔT). In addition, according to the Thomson-Gibbs equation,[47] crystal thickness (l_c), and melting temperature (T_m) are correlated as in eq. (4):

$$T_m = T_m^\circ\left(1 - \frac{2\sigma}{1_c\rho_c\Delta H}\right) \tag{4}$$

where T_m^0 is the equilibrium melting temperature, ρ_c is the mass density of the crystal, ΔH is the heat of fusion per unit weight, and σ is the fold surface free energy. From eq. (4), the bigger sizes (l_c) of crystals thus give rise to the higher T_m. Equations (3) and (4) both reveal that the small endotherm appeared at some degrees higher than the annealing temperature arises from the melting of crystals formed during the annealing.

Following the cold-crystallization peak(s) in the region of 108–130°C, there exists ongoing exothermic crystallizations (as can be seen by the raised curves relative to the baselines) before the major melting peak at near 250°C as can be seen in the total heat flow curves in Figures 1–3. In the nonreversing heat

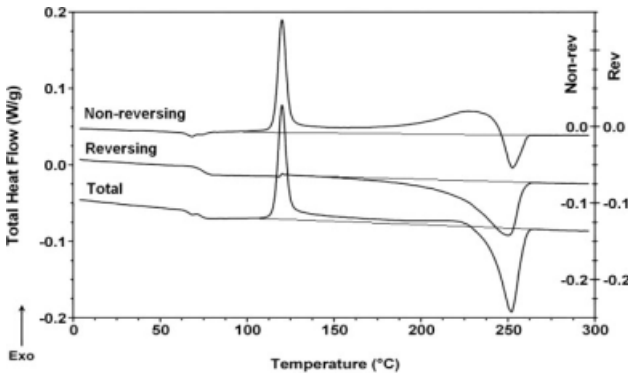

Figure 1 TMDSC curves of total, reversing, and nonreversing heat flows for aPET (amorphous PET without annealing).

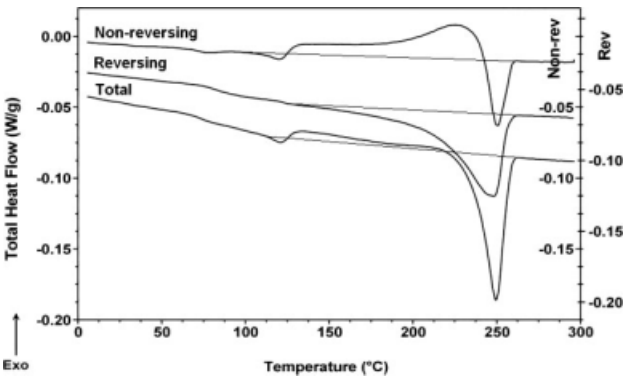

Figure 3 TMDSC curves of total, reversing, and nonreversing heat flows for aPET-110-1000 (aPET after annealing at 110°C for 1000 min).

flow curves, this ongoing exothermic crystallization can be more clearly observed and increases with increasing temperature until the major melting endotherm before which the curve evolves into an exothermic peak. This nonreversing exothermic peak is found to accompany with the reversing endothermic peak. Figure 5 shows nonreversing heat flow curves for aPET and all 110°C-annealed aPET samples. An enthalpy recovery peak (or a peak with a shoulder) around the glass transition temperatures (T_g) in the region of 70–80°C, the first and second cold-crystallization temperatures (T_{cc1},and T_{cc2}, respectively) in the region of 108–130°C, the ongoing exothermic crystallization with a peak temperature at near 227°C, and the first (minor) and second (major) melting temperatures (T_{m1} at near 120°C and T_{m2} at near 250°C, respectively) for aPET and the annealed aPET samples are observed in the nonreversing heat flow curves in Figure 5 and tabulated in Table II. The enthalpy recovery peak is associated with the enthalpy that is recovered during heating the relaxed polymer chains after the annealing treatments. Figure 5 finds that the magnitudes of the enthalpy recovery peaks increase with annealing times for samples annealed $\leq$30 min but decrease with annealing times for samples annealed $\geq$40 min. This suggests that for short annealing times ($\leq$30 min), the sample has low crystallinity (see X_d in Table I) and the relaxation of polymer chains toward an equilibrium state to have enthalpy loss is greater for longer annealing times, resulting in greater enthalpy recovery during heating. For annealing times $\geq$40 min, the low amorphous fraction because of high crystallinity (Table I) in the sample results in small enthalpy recovery peak. As can be seen in Table II, the enthalpy recovery peak temperature (T_{er}) shifts to higher temperatures for the samples with longer annealing times from 68.5°C for aPET to 75.6°C for aPET-110-1000. This can be attributed to higher degrees of crystallinity in samples of longer annealing times as can be seen in Table I.

As can be seen in Figure 5, the original aPET sample exhibits a clear cold-crystallization exotherm at 120°C during heating. The cold-crystallization exotherm shifts to lower temperatures for the annealed samples with longer annealing times within 30 min.

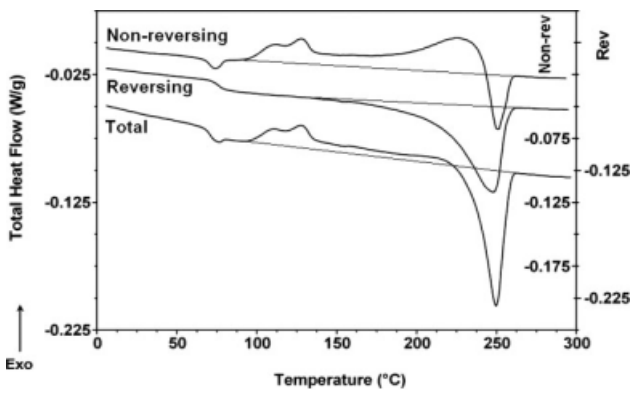

Figure 2 TMDSC curves of total, reversing, and nonreversing heat flows for aPET-110-40 (aPET after annealing at 110°C for 40 min).

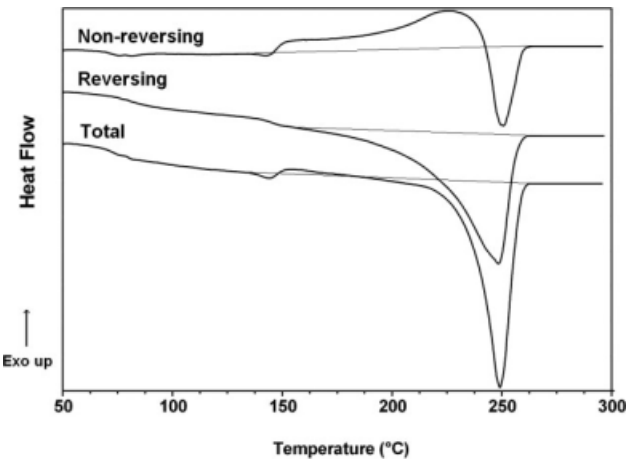

Figure 4 TMDSC curves of total, reversing, and nonreversing heat flows of aPET-140-50 (aPET after annealing at 140°C for 50 min).

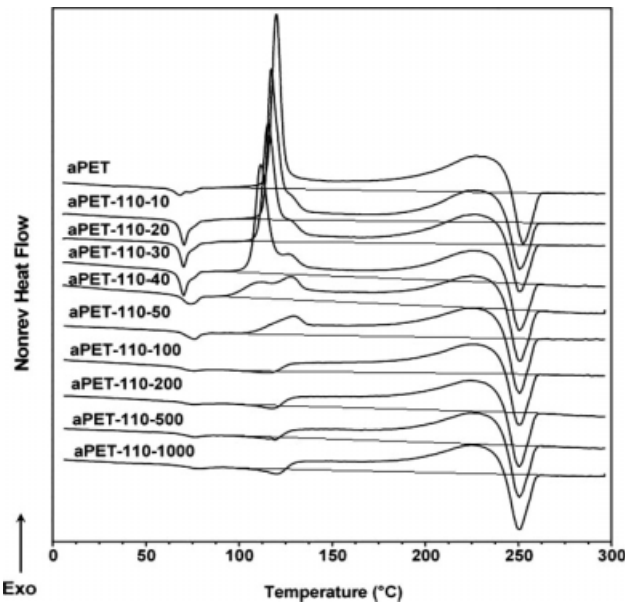

Figure 5 TMDSC curves of nonreversing heat flows for aPET and the annealed aPET at 110°C for various times.

This finding suggests that the crystals formed during annealing serve as a nucleating agent facilitating the cold-crystallization and resulting in a lowered cold-crystallization temperature. Beginning with the 10 min of annealing, a shoulder appears at the higher temperature side of the major cold-crystallization exotherm. This shoulder overlaps with the ongoing crystallization at higher temperatures. For longer annealing times, this shoulder becomes bigger accompanying with a decreasing magnitude of the major cold-crystallization peak until its complete disappearance for the samples annealed $\geq$100 min beyond which a small endotherm appears at near 120°C. This small endotherm appears to be increasing in magnitude with increasing annealing time. The origin of this small endotherm was attributed to the melting of crystals formed during annealing as discussed previously. By examining the position of the double cold-crystallization peaks (or a major peak with a shoulder) and that of the small melting peak in these nonreversing heat flow curves in Figure 5, it can be suggested that the double cold-crystallization exotherms arise from a superposition of the exothermic cold-crystallization peak and the endothermic melting peak. The original aPET undergoes no annealing treatment and has no initial crystals present to melt simultaneously with the cold-crystallization during heating. The observation of a single cold-crystallization exotherm for the original aPET thus agrees with the finding.

More evidence can be provided by DMA analysis for the origin of the double cold-crystallization exotherms. Figure 6 shows the storage modulus of aPET and the annealed samples as a function of temperature. In Figure 6, the storage modulus can be seen to decrease slowly as the temperature increases up to the onset of the glass relaxation, and then drops abruptly during the glass relaxation, as expected. As can be seen in Figure 6, the glass relaxation of sample shifts to higher temperatures for samples with longer annealing times. This is because the longer annealing times result in higher degrees of crystallinity (Table I) and this crystallinity contributes to the increases of the glass relaxation. Before the onset of the glass relaxation, the storage modulus of sample ranges from about 2000 to 2500 MPa and increases with increasing annealing time. This indicates that the crystallinity of sample contributes to the increase of the storage modulus in this low-temperature region as well. For samples with annealing times $\geq$100 min, the storage modulus curves reach a plateau region after the glass relaxations. Samples with annealing times $\leq$50 min are somewhat different in storage modulus curves after the glass relaxations due to occurrence of cold-crystallizations

TABLE II
Temperatures of the Enthalpy Recovery Peak (T_{er}), the First and Second Cold-Crystallization Temperatures (T_{cc1} and T_{cc2}, Respectively), the Ongoing Crystallization Peak Temperatures (T_{oc}), the First and Second Melting Temperatures (T_{m1} and T_{m2}, Respectively) for aPET and the Annealed aPET Samples

PET samples	T_g (°C)	T_{er} (°C)	T_{cc1} (°C)	T_{m1} (°C)	T_{cc2} (°C)	T_{oc} (°C)	T_{m2} (°C)
aPET	74.5	68.5	120.0	–	–	228.5	252.0
aPET-110-10	74.5	69.0	117.4	–	129.2	227.5	250.1
aPET-110-20	74.5	69.5	115.7	–	128.5	227.0	249.9
aPET-110-30	74.8	70.5	110.7	–	127.7	227.0	249.9
aPET-110-40	78.0	74.5	108.5	–	127.7	227.0	249.9
aPET-110-50	79.1	75.0	–	–	128.6	227.0	249.8
aPET-110-100	81.0	75.0	–	118.1	–	227.0	249.8
aPET-110-200	81.5	75.0	–	119.3	–	227.0	249.8
aPET-110-500	81.5	75.1	–	118.8	–	227.0	249.8
aPET-110-1000	81.5	75.6	–	121.1	–	227.0	249.8

These thermal properties were obtained from TMDSC nonreversing heat flow curves. The glass transition temperatures (T_g) were obtained from TMDSC reversing heat flow curves.

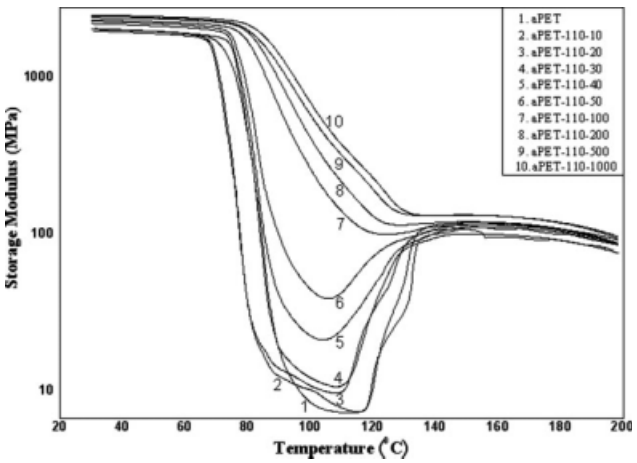

Figure 6 DMA curves of storage modulus as a function of temperature for aPET and the annealed aPET at 110°C for various times. DMA analyses were conducted at a heating rate of 3°C/min from 30 to 200°C and at an oscillation frequency of 1 Hz with an oscillation amplitude of 15 μm.

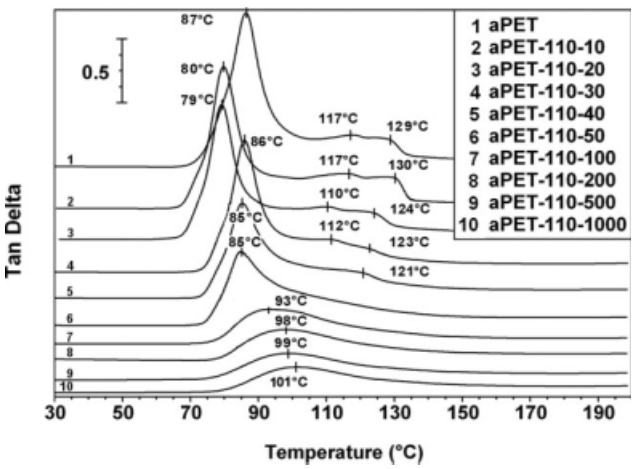

Figure 8 DMA curves of tan δ as a function of temperature for aPET and the annealed aPET at 110°C for various times.

during the DMA heating. The storage modulus of these samples annealed ≤50 min decreases rapidly during the glass relaxation to a very low value and increases with temperature in the region of 110–140°C as can been seen in Figure 6. To examine this temperature region carefully, Figure 6 is zoomed in the region of 100–150°C for aPET-110-10. The zoomed region is shown in Figure 7 where the storage modulus can be seen to increase with temperature by a two-stage process. The storage modulus begins to rise at near 120°C with a slower increasing rate and changes to a higher increasing rate at near 130°C. The slower increasing rate in the initial stage can be associated with the superposition of the melting of crystals (formed during the 10-min annealing) and the cold-crystallization during the DMA heating. In other words, the melting of crystals offsets

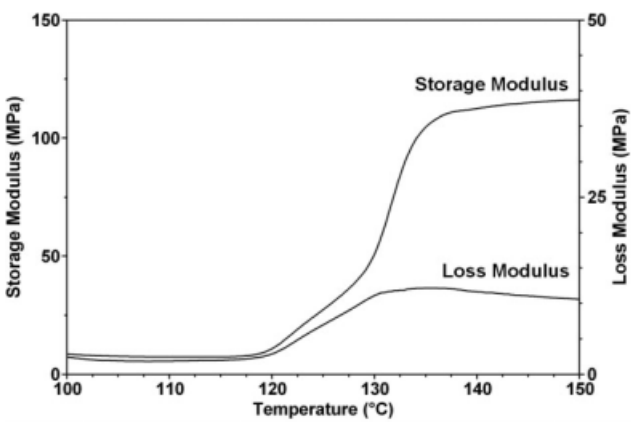

Figure 7 DMA curves of storage and loss modulus as a function of temperature for aPET-110-10.

the effect of the cold-crystallization which can give rise to an increase of storage modulus during the DMA heating. The cold-crystallization alone contributes to the increase of storage modulus on the DMA heating in the later stage and results in a higher increasing rate in the storage modulus with temperature. The melting of crystals can be also evidenced by the increase of loss modulus in the region of 120–130°C as can be also seen in Figure 7. The finding from these DMA data agree with the observation in Figure 5 as discussed previously.

The double cold-crystallization behavior can also be observed from DMA tan δ curves as a function of temperature. Figure 8 shows tan δ curves of aPET and the annealed aPET samples as a function of temperature. Every sample exhibits a major relaxation (or damping) peak attributed to the glass transition. For the samples with longer annealing times, the major damping peak shifts to higher temperatures and becomes smaller in magnitude. This can be attributed to higher degrees of crystallinity. For samples with short annealing times (<50 min), two or one small and broad additional damping peaks appear at temperatures higher than the glass transition peak as can be seen in Figure 8. Compared with TMDSC nonreversing curves in Figure 5, the small and broad damping peaks in Figure 8 are qualitatively consistent with the cold-crystallization peaks in Figure 5. Although double cold-crystallization exotherms are not seen for aPET in Figure 5 because of relatively low sensitivity from the TMDSC analysis compared with the DMA analysis, the appeared two small additional damping peaks for aPET in Figure 8 can serve as evidence that the melting of crystals occurs during the cold-crystallization. These crystals are formed in aPET during the cold-

crystallization by DMA heating. Overall, the tan δ data support the finding from TMDSC data that the melting of crystals, formed by the annealing process, superposes with the cold-crystallization occurring during heating on the annealed samples. This superposition gives double cold-crystallization peaks for samples with low degrees of crystallinity. The samples with high degrees of crystallinity exhibit no cold-crystallization peak(s) but exhibit a melting peak nearby.

CONCLUSIONS

The enthalpy recovery peak in the glass transition region, the double cold-crystallization peaks, and the ongoing crystallization after the cold crystallization in the 110°C-annealed amorphous PET samples with different crystallinity were clearly observed in the TMDSC nonreversing heat flow curves. The enthalpy recovery peak was found to shift to higher temperatures for samples with higher degrees of crystallinity. The magnitudes of the enthalpy recovery peaks were found to increase with annealing times for samples annealed $\leq$30 min but to decrease with annealing times for samples annealed $\geq$40 min. The TMDSC nonreversing curves also found that the annealed aPET samples with low crystallinity exhibited double cold-crystallization peaks (or a major peak with a shoulder) in the region of 108–130°C, whereas the annealed samples with high crystallinity exhibited one small or no cold-crystallization peak. The double cold-crystallization exotherms in samples of low crystallinity could be attributed to the superposition of the melting of crystals, formed by the annealing process, and the cold-crystallizations during TMDSC heating. DMA data agreed with the TMDSC data.

References

1. Mark, H. F.; Bikales, N. M.; Overberger, C. G.; Menges, G.; Kroschwits, J. I. Encyclopedia of Polymer Science and Engineering, 2nd ed.; Wiley: New York, Vol. 12, 1988.
2. Zhou, C.; Clough, S. B. Polym Eng Sci 1988, 28, 65.
3. Kitano, Y.; Kinoshita, Y.; Ashida, T. Polymer 1995, 36, 1947.
4. Okazaki, I.; Wunderlich, B. J Polym Sci Part B: Polym Phys 1996, 34, 2941.
5. Wang, Z. G.; Hsiao, B. S.; Sauer, B. B.; Kampert, W. G. Polymer 1999, 40, 4615.
6. Bashir, Z.; Al-Aloush, I.; Al-Raqibah, I.; Ibrahim, M. Polym Eng Sci 2000, 40, 2442.
7. Tan, S.; Su, A.; Li, W.; Zhou, E. J Polym Sci Part B: Polym Phys 2000, 38, 53.
8. Alves, N. M.; Mano, J. F.; Balaguer, E.; Meseguer Duenas, J. M.; Gomez Ribelles, J. L. Polymer 2002, 43, 4111.
9. Kiflie, Z.; Piccarolo, S.; Brucato, V.; Balta-Calleja, F. J. Polymer 2002, 43, 4487.
10. Avila-Orta, C. A.; Medellin-Rodriguez, F. J.; Wang, Z. G.; Navarro-Rodriguez, D.; Hsiao, B. S.; Yeh, F. Polymer 2003, 44, 1527.
11. Bartolotta, A.; Di Marco, G.; Farsaci, F.; Lanza, M.; Pieruccini, M. Polymer 2003, 44, 5771.
12. Minakov, A. A.; Mordvintsev, D. A.; Schick, C. Polymer 2004, 45, 3755.
13. Rastogi, R.; Vellinga, W. P.; Rastogi, S.; Schick, C.; Meijer, H. E. H. J Polym Sci Part B: Polym Phys 2004, 42, 2092.
14. Androsch, R.; Wunderlich, B. Polymer 2005, 46, 12556.
15. Sorrentino, L.; Iannace, S.; Di Maio, E.; Acierno, D. J Polym Sci Part B: Polym Phys 2005, 43, 1966.
16. Vyazovkin, S.; Stone, J.; Sbirrazzuoli, N. J Therm Anal Calorim 2005, 80, 177.
17. Sirelli, L.; Pereira, R. A.; Perez, C. A.; Dias, M. L. J Macromol Sci Phys 2006, 45, 343.
18. Kawakami, D.; Ran, S.; Burger, C.; Avila-Orta, C.; Sics, I.; Chu, B.; Hsiao, B. S.; Kikutani, T. Macromolecules 2006, 39, 2909.
19. Ellis, J. W.; Picot, J. J. C. Polym Eng Sci 2000, 40, 1619.
20. Maruhashi, Y. Polym Eng Sci 2001, 41, 2194.
21. Zumailan, A.; Dargent, E.; Saiter, J. M. Polym Eng Sci 2004, 44, 223.
22. Zhao, J.; Song, R.; Zhang, Z.; Linghu, X.; Zheng, Z.; Fan, Q. Macromolecules 2001, 34, 343.
23. Zhao, J.; Wang, J.; Li, C.; Fan, Q. Macromolecules 2002, 35, 3097.
24. Bosma, M.; Brinke, G.; Ellis, T. Macromolecules 1988, 21, 1465.
25. Wang, Y.; Gomez Ribelles, J. L.; Salmeron Sanchez, M.; Mano, J. F. Macromolecules 2005, 38, 4712.
26. Surana, R.; Pyne, A.; Rani, M.; Suryanarayanan, R. Thermochim Acta 2005, 433, 173.
27. McGonigle, E. A.; Jenkins, S. D.; Liggat, J. J.; Pethrick, R. A. Polym Int 2000, 49, 1458.
28. McGonigle, E. A.; Daly, J. H.; Gallagher, S.; Jenkins, S. D.; Liggat, J. J.; Olsson, I.; Pethrick, R. A. Polymer 1999, 40, 4977.
29. McGonigle, E. A.; Daly, J. H.; Gallagher, S.; Jenkins, S. D.; Liggat, J. J.; Olsson, I.; Pethrick, R. A.; Jenkins, S. D.; Liggat, J. J.; Pethrick, R. A. Macromolecules 2000, 33, 480.
30. Vigier, G.; Tatibouet, J.; Benatmane, A.; Vassoille, R. Colloid Polym Sci 1992, 270, 1182.
31. Cortes, P.; Montserrat, S. J Polym Sci Part B: Polym Phys 1998, 36, 113.
32. Montserrat, S.; Cortes, P. J Mater Sci 1995, 30, 1790.
33. Li, Q.; Simon, S. L. Polymer 2006, 47, 4781.
34. Kampert, W.G.; Sauer, B. B. Polymer 2001, 42, 8703.
35. Sauer, B. B.; Kampert, W. G.; Neal Blanchard, E.; Threefoot, S. A.; Hsiao, B. S. Polymer 2000, 41, 1099.
36. Gill, P. S.; Sauerbrunn, S. R.; Reading, M. J Therm Anal 1993, 40, 931.
37. Okazaki, I.; Wunderlich, B. Macromolecules 1997, 30, 1758.
38. Okazaki, I.; Wunderlich, B. Macromol Rapid Commun 1997, 18, 313.
39. Wunderlich, B. Prog Polym Sci 2003, 28, 383.
40. Daubeny, R.; Bunn, C. W.; Brown, C. J. Proc R Soc 1954, A226, 531.
41. Mayhan, K. G.; James, W. J.; Bosch, W. J Appl Polym Sci 1965, 9, 3605.
42. Fischer, E. W.; Fakirov, S. J Mater Sci 1976, 11, 1041.
43. Mehta, A.; Gaur, U.; Wunderlich, B. J Polym Sci Part B: Polym Phys 1978, 16, 289.
44. Blundell, D. J.; Osborne, D. N. Polymer 1983, 24, 953.
45. Hoffman, J. D.; Weeks, J. J. J Res Natl Bur Stand A Phys Chem 1962, 66A, 13.
46. Hoffman, J. D.; Miller, R. L. Polymer 1997, 38, 3151.
47. Gedde, U. W. Polymer Physics; Chapman & Hall: New York, 1995.